Photovoltage-induced blockade of charge and spin diffusion in semiconducting thin films

S. Park, D. Paget, V. Berkovits, V. Ulin, P. Alekseev, N. Kaliuzhnyi, S. Mintairov, F. Cadiz

Photovoltage-induced blockade of charge and spin diffusion in semiconducting thin films

S. Park[1], D. Paget[1], V. L. Berkovits[2], V. P. Ulin[2], P. A. Alekseiev[2], N. A. Kalyuzhnyi[2], S. A. Mintairov[2], and F. Cadiz[1]
[1]*Physique de la matière condensée, Ecole Polytechnique, CNRS, Université Paris Saclay, 91128 Palaiseau, France and*
[2]*Ioffe Institute, Saint Petersburg, Russia.*
(Dated: December 20, 2018)

In semiconductors under tightly-focused photocarrier excitation, the lateral variation of carrier concentration induces a lateral variation of photovoltage. In p-type GaAs films at 300K, it is shown experimentally and theoretically that the photovoltage lateral dependence is able to block the photoelectron diffusion, thus reducing the effective charge diffusion constant by a factor of ≈ 5 with respect to surface-free conditions. The photovoltage lateral variation also induces a coupling between charge and spin diffusion . Because of this coupling, the effective spin diffusion constant is significantly larger than the effective charge one.

PACS numbers:

I. INTRODUCTION

In the context of future active spintronic devices, the diffusion of charge and spin in semiconductors have been investigated by numerous authors. For most of these studies, a tightly-focused laser or electron beam locally generates photoelectrons and the spatial distribution of charge and spin is monitored, using cathodoluminescence [1], time-resolved [2], steady-state photoluminescence [3, 4], or magneto-optical detection [5–7]. If the electrons are not confined by a semiconducting overlayer of larger bandgap, it has been found that the diffusion length increases with surface passivation because of the decrease of surface recombination, so that its experimental determination has been used to obtain the value of the surface recombination velocity [8].

The present work is a theoretical and experimental investigation of the effect of photovoltage on lateral charge and spin transport. This photovoltage is tuned by surface chemical treatment of the sample and by changing the light excitation power. For a tightly-focused excitation, the surface photovoltage is larger near the excitation spot than at some distance from this spot. Thus, there appears an electric field parallel to the surface which can completely block the lateral carrier diffusion and thus strongly perturb the investigation of charge and spin transport. For a p-type GaAs film, in the whole distance range near the excitation spot where the photovoltage is larger than the thermal energy, a chemical passivating treatment has a negligible effect on the diffusion length. The effect of this passivation only manifests itself at larger distances at which the smaller surface photovoltage no longer blocks the photoelectron diffusion. Furthermore, the surface photovoltage lateral variation is shown to induce a spin-charge coupling. This coupling also decreases the spin diffusion length. But this decrease is significantly smaller than for the charge so that the effective charge and spin diffusion lengths are comparable, in spite of an efficient spin relaxation. This implies that the spin diffusion constant is larger than the charge one.

II. EXPERIMENTAL

A. Results

We have used MOCVD-grown structures composed of a 3μm-thick p-type GaAs film (zinc doping $N_A = 10^{17}$ cm^{-3}), grown on a semi-insulating substrate, with an interfacial $Ga_{0.6}Al_{0.4}As$ layer in order to confine the photoelectrons. Three samples were investigated: a) a naturally-oxidized piece of the sample. b) An identical sample, covered by a 100 nm-thick layer of $Ga_{0.6}Al_{0.4}As$. c) A piece of the same wafer obtained by treating the oxidized surface for 10 min. by a saturated sodium sulfide solution. This treatment is known to saturate Ga surface dangling bonds by sulfur atoms, and to reduce S by about one order of magnitude [9]. It will be shown in the supplementary information that the photovoltage is negligible for the oxidized and encapsulated samples, while it can be significant for the passivated sample. This sample will allow us to reveal the induced effect on charge and spin transport.

As described in Ref. [3], the sample is excited by a tightly-focused, continuous laser beam (Gaussian radius $\sigma \approx 0.6$ μm, energy 1.59 eV). The emitted light is focused on the entrance slit of a spectrometer equipped with a CCD camera as a detector. For a very low excitation power of 300 nW, an image given by this camera is shown in Panels a and b of Fig. 1 for the $Ga_{0.6}Al_{0.4}As$-encapsulated and oxidized sample, respectively. For such image, the x coordinate contains the spectral information while the y coordinate reveals the spatial profile along a line on the sample defined by the spectrometer entrance slit. Addition of the values of all the pixels corresponding to the same wavelength allows us to obtain the spatially-unresolved luminescence spectrum. The corresponding spectra are shown in Panel c of Fig. 1. As expected,

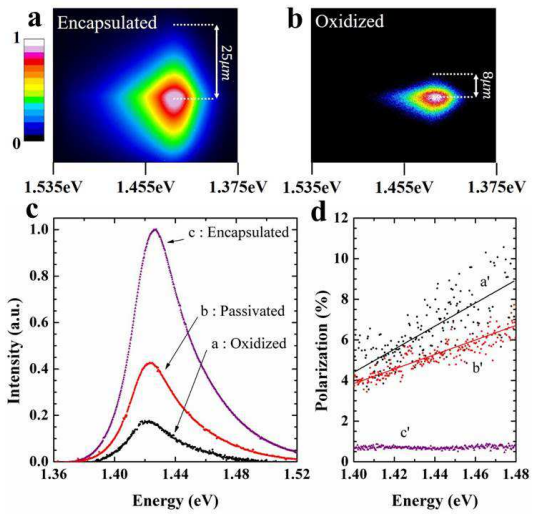

FIG. 1: Panels and and b show the PLI images at 300K, for an excitation power of 300 nW, obtained from the CCD at the spectrometer output, for the encapsulated and the oxidized samples, respectively. Integration of these images along a vertical axis gives the spatially-unresolved luminescence spectra, shown in Curve a of panel c for the oxidized surface, Curve b for the sulfur-passivated one and Curve c for the GaAlAs-encapsulated one. The corresponding spectra of the degree of circular polarization are shown in Panel d.

because of the significant surface recombination of the oxidized surface, the peak intensity of the corresponding sample is smaller than for the $Ga_{0.6}Al_{0.4}As$-encapsulated one by a factor 5.9. The PL peak intensity of the sulfide-passivated sample is larger than for the oxidized sample by a factor of 2.5, which evidences the decrease of S brought by this treatment [9].

Liquid crystal modulators are used to excite the sample with $\sigma^{\pm}$-polarized light. This generates a nonzero spin density $s = n_+ - n_-$, where $n_{\pm}$ are the concentrations of electrons with spin $\pm 1/2$, choosing the z direction as the quantization axis. For a given helicity of light excitation, the $\sigma^{\pm}$-polarized components of the luminescence, of intensity $I(\sigma^{\pm})$ are selectively measured. The difference signal $I_D = I(\sigma^+) - I(\sigma^-)$ is proportional to the spin orientation $s = n_+ - n_-$, while the sum signal $I_S = I(\sigma^+) + I(\sigma^-)$ is proportional to the electronic concentration orientation $n = n_+ + n_-$.

Panel d of Fig. 1 shows the spectra of the luminescence degree of circular polarization $\mathscr{P} = I_D/I_S = 0.5s/n$ for the three samples. Because of its long effective lifetime, the encapsulated sample (Curve c') exhibits a very small polarization of 0.5%. For the two other samples, the polarization is larger for above bandgap luminescence energy, revealing as is frequently observed, the increased polarization of electrons with increased kinetic energy. The largest polarization, of 5% at the luminescence peak, is obtained for the oxidized sample, because of the relatively small losses of spin orientation caused by the shorter lifetime. As expected, the polarization of the sulfidized sample, of 4.5%, is smaller than for the oxidized surface because of its longer lifetime.

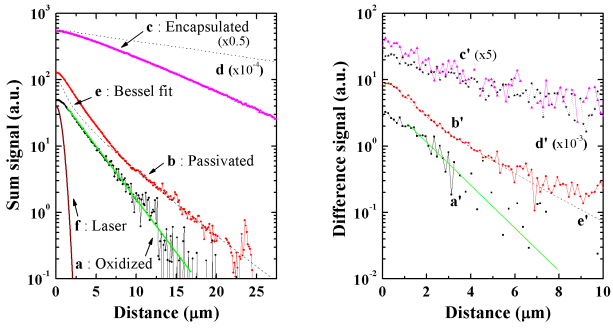

FIG. 2: The left panel shows the spatial profiles of the luminescence intensities at 300K and an excitation power of 300nW, for the oxidized surface (Curve a), the sulfur-passivated one (Curve b), and the GaAlAs-encapsulated one (Curve c). The dotted line shown in Curve d is the normalized profile for the same sample at a maximum power of 1 mW. Also shown is the laser spatial profile (Curve f), and an attempt to fit Curve b using Eq. (3) (Curve e). The right panel shows the spatial profiles of the difference signal, revealing the spin orientation spatial profile, for the oxidized surface (Curve a') , the sulfur-passivated one (Curve b') and the GaAlAs-encapsulated one (Curve c') including the corresponding profile at 1mW (Curve d'). Curve e', calculated using Eq. (3), correctly interprets the spatial profile.

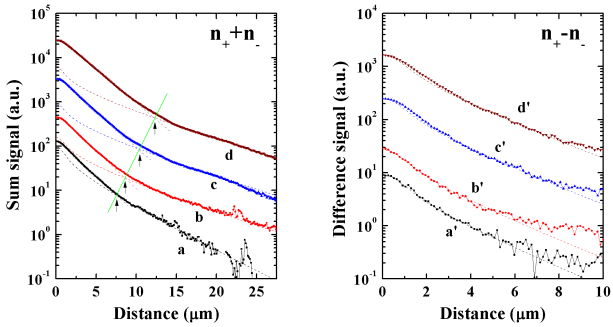

FIG. 3: The left panel shows the spatial profiles of the luminescence intensity for the passivated sample for increased excitation powers: 300 nW (Curve a, same as Curve b of Fig. 2), 1.2 μW (Curve b), 8.5 μW (Curve c), 40 μW (Curve d). The right panel shows the corresponding profiles of the difference signal. In the two panels, dotted curves represent fits of the profiles using Eq. (3)

The charge profiles, obtained from a cut along the y axis of the images shown in Fig. 1 at the energy of the PL maximum, are shown in the left panel of Fig. 2. As shown in Curve c, for the nearly surface-free $Ga_{0.6}Al_{0.4}As$-encapsulated sample, one obtains $L_c \approx 8$ μm. This large value is however affected by a residual surface recombination, since the increase of excitation power, known to reduce the surface recombination velocity [8], induces a further increase of diffusion length (Curve d, taken for 1mW), which is now equal to 24.4 μm. This value will be in the following taken for the surface-

free charge diffusion length. For the oxidized sample, as found from Curve a of Fig. 2, the diffusion length is ≈ 2.6 μm.

The spatial profiles of the spin orientation, shown in the right panel of Fig. 2, reveal a similar behavior. The effective spin diffusion length is ≈ 5.8 μm for the encapsulated surface (Curve d') and ≈ 2.1 μm for the oxidized one (Curve a').

For the passivated sample, as seen in Curve b, the charge spatial profile exhibits two steps. Up to $r = 7$ μm, in contradiction with the passivation-induced luminescence increase, one finds a diffusion length of $\approx 2.45 \pm 0.3$ μm i. e. sligthly smaller than for the oxidized sample, while at a larger distance, one finds a value of ≈ 5.2 μm. It is pointed out that such excess signal induced by surface passivation at low distance is visible in previous work (see Curve b of Fig. 3 in Ref. [8]), although the profile is only analyzed at larger distance.

Curve b' of Fig. 2 shows that, for $r > 3$ μm, the spin diffusion length is $\approx 2.9 \pm 0.3$ μm i. e. comparable to the charge diffusion length in the same spatial range in spite of the efficient spin relaxation. Note that the measurement accuracy for this very small excitation power and this relatively small spin polarization is not sufficient to obtain a reliable value of the spin diffusion length for $r > 7$ μm. The various values of charge and spin diffusion lengths are summarized in Table I.

We have investigated the effect of excitation power on the spatial profile of the passivated sample. This power is kept to a value smaller than the value at which ambipolar diffusion and bimolecular recombination start to perturb the profile for an encapsulated sample [10] so that, for the passivated sample for which the photoelectron concentration is smaller, these effects will be considered as negligible. As seen from the right panel of Fig. 3, the amplitude of the step at small distance of the charge profile strongly increases with the excitation power while the corresponding diffusion length sligthly increases to 2.53 μm (Curve b), 2.62 μm (Curve c) and 2.86 μm (Curve d). The position of the crossover, marked by arrows in the figure shifts to larger distances, and the diffusion length after the crossover increases to 8.9 μm (Curves b, c, and d), Conversely, the spin diffusion profile weakly changes, with a slight increase of the spin diffusion length which is 3.1 μm (Curve b'), 3.2 μm (Curve c') and 3.3 μm (Curve d').

B. Interpretation without photovoltage

The charge profile is quite generally described by the diffusion equation

$$0 = g(r,z)\tau^* - n + \frac{\tau^*}{q}\vec{\nabla}\cdot\overrightarrow{J}_c, \qquad (1)$$

where the generation rate is of the form $g(r,z) = \alpha g_0 \exp[-\alpha z - (r/\sigma)^2]$ where α is the light absorption coefficient, r is the distance to the excitation spot, z is the distance to the sample surface and q is the absolute value of the electron charge. The charge diffusive current is equal to $\overrightarrow{J}_c = qD_e\vec{\nabla}n$, where D_e is the diffusion constant. The time τ^* is the effective photoelectron lifetime including the surface. Including recombination at the front surface of velocity S and neglecting the recombination at the back interface, it is given by [8]

$$\frac{1}{\tau^*} = \frac{1}{\tau} + D_e\frac{\theta^2}{d^2}, \qquad (2)$$

Here d is the sample thickness and θ is the solution of $\theta\tan(\theta) = Sd/D_e$. This equation has solutions corresponding to $(k-1)\pi/2 < \theta < k\pi/2$. However, in a 2-dimensional picture, i. e. assuming that $Sd/D_e << 1$, only the fundamental solution corresponding to $k = 1$ will be considered. The luminescence profile is given by [4]

$$I(r) \propto \int_0^\infty K_0(\frac{r'}{L_c^*})e^{-(r-r')^2/\sigma^2}dr' \qquad (3)$$

where K_0 is the modified Bessel function of the second kind and $L_c^* = \sqrt{D_e\tau^*}$. Finally, the overall luminescence intensity, obtained by performing an integral over r and z in the same way as used elsewhere [11], is given by

$$I \propto \frac{g}{\alpha L_c}\left\{\frac{A}{B} - \frac{1}{\alpha L_c}\left[e^{-\alpha d}(\alpha^2 L_c^2 - 1) + 1\right]\right\}, \qquad (4)$$

where

$$A = \gamma\left[\sinh(d/L_c) + \alpha L_c e^{-\alpha d}\right] + \alpha L_c \sinh(d/L_c), \qquad (5)$$

$$B = \gamma\cosh(d/L_c) + \sinh(d/L_c), \qquad (6)$$

where $\gamma = SL_c/D_e$. The spin diffusion equation is

$$0 = g(r,z)\tau_s^*\mathscr{P}_i - s + \frac{\tau_s^*}{q}\vec{\nabla}\cdot\overrightarrow{J}_s, \qquad (7)$$

where $\mathscr{P}_i = \mp 0.5$ for a $\sigma^\pm$ helicity of the excitation light, and the spin lifetime τ_s^* is given by $1/\tau_s^* = 1/\tau^* + 1/T_1$, where T_1 is the spin relaxation time. The spin diffusive current is $\overrightarrow{J}_s = qD_e\vec{\nabla}s$ and the spin spatial profile is

TABLE I: Measured values, in μm units, of the bulk charge (L_c) and spin diffusion lengths (L_s), of the effective photovoltage-free charge (L_c^*) and spin (L_s^*) diffusion lengths and of the corresponding quantities ($\mathscr{L}_c$ and $\mathscr{L}_s$, respectively), affected by the photovoltage that is, for the passivated sample and $r < 7$ μm.

sample	L_c	L_s	L_c^*	L_s^*	$\mathscr{L}_c$	$\mathscr{L}_s$
Encapsulated	24.4	5.8	-	-	-	-
Oxidized	-	-	2.6	2.12	-	-
Passivated ($r > 7$ μm)	-	-	5.2	-	-	-
Passivated ($r < 7$ μm)	-	-	-	-	2.45	2.9

determined by an equation similar to Eq. (3), where the spin diffusion length is $L_s^* = \sqrt{D_e \tau_s^*}$.

For the encapsulated sample, the time τ^* is equal to the bulk lifetime τ and the surface-free charge and spin diffusion lengths are equal respectively to $L_c = \sqrt{D_e \tau} = 24.4$ μm and $L_s = \sqrt{D_e \tau_s} = 5.8$ μm, where $1/\tau_s = 1/\tau + 1/T_1$. Taking for the bulk recombination time $\tau = 30$ ns, which has been measured for the same doping [10, 12], one obtains $D_e = 200$ cm^2/s and $T_1 = 1.8$ ns, a value which is close to the value found in the literature [13]. These values are probably accurate within 20% and will be used to semi-quantitatively model the results for the other samples.

For the oxidized sample, using the measured value of L_c^*, the above values of D_e and τ and Eq. (2), we obtain $S \approx 1.7 \times 10^6$ cm/s, a value close to that of 3×10^6 cm/s obtained previously for oxidized GaAs [8]. This gives $\tau^* = 0.34$ ns and finally allows us to predict a value of the spin diffusion length L_s^* of 2.38 μm, close to the observed value of 2.2 μm. It is concluded that, for the oxidized and encapsulated samples, the results are fully consistent with a photovoltage-free picture.

For the passivated sample, the spatial profiles for $r > 7$ μm are also correctly interpreted by the photovoltage-free model, because the photovoltage is negligible for the weak photoelectron concentration in this spatial range. From the passivation-induced increase of the PL intensity and using Eq. (4), we obtain $S = 3 \times 10^5$ cm/sec that is, a factor 5 smaller than for the oxidized surface. This allows us to predict an increased diffusion length of the passivated sample of $L_c^* \approx 4.3$ μm, close to the experimental value of $L_c^* \approx 5.2$ μm. The increase with power of the charge diffusion length at large distance, shown in Fig. 3, reflect the power dependence of S, which is known to decrease for an increasing excitation power and to increase the charge and spin lifetimes [8].

However, the present picture fails to interpret the spatial profiles of the passivated sample for $r < 7$ μm. As seen in the left panel of Fig. 3 and Curve e of Fig. 2, the charge profile cannot be interpreted using Eq. (3), which predicts only one step in the decay. If one rather considers 3D diffusion, an additional signal is predicted to appear near $r = 0$, because of a spatial mode of higher order [4]. However, we calculate that such mode is negligible : it only extends up to $r = 2$ μm and its intensity is smaller than 3% of the main mode. Moreover, the excess signal near $r = 0$ cannot be attributed to such a mode, since its intensity is predicted to increase upon increasing S and should be larger for the oxidized sample than for the passivated one. Note that the spin spatial profile can be interpreted using Eq. (3) and a slightly increased value of $\sigma = 0.8$ μm which may account for diffusion of carriers during thermalization (right panel of Fig. 3). However the spin diffusion length, of value 2.9 μm at low excitation power, is within measurement accuracy comparable with the charge diffusion length in the same spatial range, in contradiction with the expected decrease of the spin lifetime caused by spin relaxation.

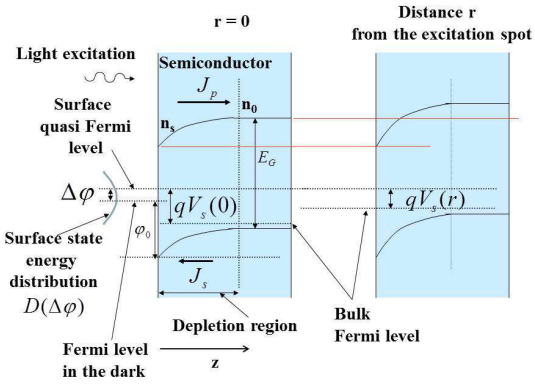

FIG. 4: Schematic representations of the band structure of the photo-excited GaAs film. The left panel corresponds to the place of light excitation and shows the surface electron quasi Fermi level, shifted from its position in the dark by $\Delta\varphi$, and the photovoltage value $qV_s(0)$. In comparison, the right panel, showing the 2-dimensional band structure at distance r from the laser spot, shows a smaller photovoltage $qV_s(r)$. Because of the screening by the large subsurface photoelectron concentration n_s, the positions of the conduction and valence band at the surface do not depend on r, so that the photovoltage spatial dependence only concerns the band energy in the bulk region near the onset of the depletion region. The resulting electric field in the surface plane blocks the diffusion of photoelectrons in the plane parallel to the surface. Also shown are the photocurrent J_p and the Schottky current J_s, the barrier in the dark φ_0 and the width of the depletion zone W.

III. THEORY

Fig. 4 shows the subsurface band structure at the place of excitation (left panel) and at some distance r away from this place (right panel), assuming that there exists at all distances from the laser spot a local thermodynamic equilibrium between bulk and surface. This figure defines the photoinduced Fermi level unpinning $\Delta\varphi$, the surface barrier φ_B and the photovoltage V_s [11]. The strong lateral variation of V_s induced by the lateral variation of the photoelectron concentration is shown here to block the outward diffusion of photoelectrons.

The photovoltage lateral variation may affect i) the position of the conduction band at the surface in which case it will be screened by the current of photoelectrons in the depletion layer, or ii) at the beginning of the depletion zone ($z = W$) in which case it will be screened by currents of photoelectrons or of dark holes in the bulk. However, the ratio n_s/n_0 of the electron concentration at the surface and at $z = W$, assuming equilibrium between bulk and surface, is of the order of $\exp(\varphi_B/k_BT)$. Here, φ_B is the surface barrier and k_B is Boltzmann's constant [11]. This evaluation is approximate since it neglects the possible quantization in the conduction band and the modification of the shape of the conduction band in the z direction by the photoelectrons near the surface. However, one may conclude that because of the very large value of

n_s/n_0, the lateral conductance of the depletion zone is higher than that of the photoelectrons and holes in the bulk by several orders of magnitude. Thus, screening is much more efficient at the surface than in the bulk, which implies that the photovoltage spatial variation manifests itself as a spatial change of the conduction band in the semiconductor bulk. Since the energy of the bottom of the conduction band at $r = 0$ is be lower than at distance r, there results an electric field $\vec{E}^{pv}$ parallel to the surface which opposes to the diffusive current. The resulting drift current, in the plane parallel to the surface situated at the onset of the depletion region, is given by

$$\vec{J}_c^{pv} = q\mu_e n_0 \vec{E}^{pv} = -q\mu_e n_0 \frac{\partial V_s}{\partial n_0} \vec{\nabla}_r n_0, \qquad (8)$$

where μ_e is the electron mobility and n_0 is the photoelectron concentration at the onset of the depletion region. In order to calculate $\partial V_s/\partial n_0$, it is assumed that the injected photocurrent J_p and the Schottky current J_s are locally equal for all values of r. This is because the width of the depletion region $W \approx 100$ nm is much smaller than the characteristic length of the lateral photovoltage variation ($L_c^* \approx 2$ μm). One has [11]

$$qn_0 S = J_0 e^{-\frac{\Delta\varphi}{k_B T}} [e^{\frac{qV_s}{k_B T}} - 1], \qquad (9)$$

where the saturation current J_0 is related to the surface barrier in the dark φ_0 by $J_0 = A^{**}T^2 \exp(-\varphi_0/k_B T)$. Here, S is of the form

$$S = S_0 \exp(-\frac{\Delta\varphi}{k_B T})/D(\Delta\varphi), \qquad (10)$$

where $D(\Delta\varphi)$, shown in the left panel of Fig. 5, is the relative density of surface states, with respect to that at the Fermi level in the dark. One obtains then

$$\frac{\partial V_s}{\partial n_0} = \frac{1}{n_0}\frac{k_B T}{q}\xi, \qquad (11)$$

where the quantity ξ is given by

$$\xi = 1 - \exp\left[-\frac{qV_s}{k_B T}\right] = \frac{1}{1 + J_0 D(\Delta\varphi)/(qn_0 S_0)}, \qquad (12)$$

Using Eq. (8) and Einstein's relation, the outward photovoltage-induced current at the onset of the depletion region has the following form

$$\vec{J}_c^{pv} = -qD_e \xi \vec{\nabla}_r n_0. \qquad (13)$$

Adding in Eq. (1) this current to the usual diffusion current, one can define an effective charge diffusion length, given by $\mathscr{L}_c = \sqrt{\mathscr{D}_e \tau^*}$, where $\mathscr{D}_e = D_e(1-\xi)$ is an effective diffusion constant. An immediate outstanding consequence is that, if $qV_s > k_B T$ so that $\xi = 1$, the photovoltage-induced current no longer depends on V_s.

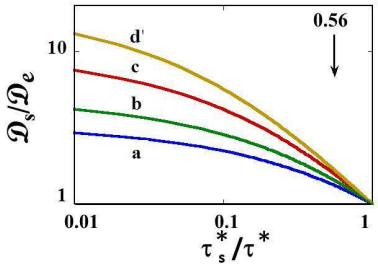

FIG. 5: Dependence of the ratio $\mathscr{D}_s/\mathscr{D}_e$ of the spin and charge diffusion constants, including the photovoltage calculated using Eq. (16), as a function of the ratio τ_s^*/τ^* of effective spin and charge lifetimes, for ξ^* equal to 0.7 (Curve a), 0.8 (Curve b, as suggested by the experiment), 0.9 (Curve c) and 0.95 (Curve d). This ratio is significantly larger than unity which implies that the photovoltage affects the spin diffusion less than the charge one. The arrow shows the estimated value of τ_s^*/τ^*.

This current exactly compensates the inward diffusion current $qD_e\vec{\nabla}_r n_0$ so that charge diffusion in the plane parallel to the surface is blocked. Assuming that this large photovoltage regime corresponds to $r < 7$ μm, this model readily explains the reduced diffusion constant at small distance for the passivated sample. We estimate $\mathscr{D}_e \approx 44$ cm^2/s that is, nearly a factor 5 smaller than D_e. Conversely, for $r > 7$ μm, one has $V_s < k_B T/q$ so that the spatial profiles are in agreement with the photovoltage-free model of the preceding section.

This picture is semi-quantitative since it considers only diffusion in the sample plane corresponding to the beginning of the space charge region and assumes that the electric field $\vec{E}^{pv}$ extends through the whole sample depth, thus neglecting majority hole currents perpendicular to the surface. Such effect should be limited since it the resulting electric field perpendicular to the surface should result in an increased photoelectron concentration near the surface and therefore an increase of the photovoltage effect. While numerical resolution of the diffusion equations in the whole sample is beyond the scope of the present work, these effects will be taken into account by using a phenomenological value of ξ, found here to be $\xi^* \approx 0.8$.

The effect of excitation power, shown in Fig. 3, can also be understood with the present model. The slope of the profiles at short distance is mostly determined by ξ^* and should indeed weakly depend on excitation power. Because of the increased photoelectron concentration, the large photovoltage regime corresponds to an increased distance range. The position of the crossover is defined by $n_0 \approx [J_0 D(\Delta\varphi)]/(qS_0)$. The increase of the PL intensity at the crossover reveals the increase of $D(\Delta\varphi)$ with power. This increase, of slightly less than 2 orders of magnitude, seems realistic since similar increases have been found on passivated GaAs surfaces for an energy change of 200 meV [14].

In the same way, the photovoltage-induced spin cur-

rent, defined as the difference between the currents of + and − spins, is given by

$$\overrightarrow{J}_s^{pv} = \overrightarrow{J}_+^{pv} - \overrightarrow{J}_-^{pv} = -q\mu_e s_0 \frac{\partial V_s}{\partial n_0} \overrightarrow{\nabla}_r n_0, \qquad (14)$$

where s_0 is the value of s near $z = W$. Using Eq. (11), one obtains

$$\overrightarrow{J}_s^{pv} = -qD_e \frac{s_0}{n_0} \xi \vec{\nabla}_r n_0, \qquad (15)$$

This equation reveals that there appears a photovoltage-induced charge-spin coupling mechanism due to which spin diffusion depends on $\overrightarrow{\nabla}_r n_0/n_0$. The modified spin diffusion equation is obtained by adding to Eq. (7) the term $(\tau_s^*/q)\overrightarrow{\nabla} \cdot \overrightarrow{J}_s^{pv}$. Provided the hole mobility μ_h can be neglected with respect to μ_e, the expression for the spin current is identical to the one found in the case of ambipolar diffusion [15], thus revealing the fundamental similarity between the spin-charge coupling induced by the two effects. In the present case, outward diffusion is slowed down by electron accumulation near the excitation spot while, for ambipolar diffusion, hole accumulation takes place. These two situations are equivalent since, because of charge neutrality, hole and electron concentrations are equal.

In the $2 < r < 7$ μm range, an effective spin diffusion length, $\mathscr{L}_s$ can be found since both I_s and I_d have exponential lateral decays. Taking $s_0 \propto \exp(-r/\mathscr{L}_s)$, the third term of Eq. (7) can be written $\mathscr{L}_s^2 \Delta s_0$, where Δ is the Laplacian operator, provided

$$\frac{\mathscr{L}_s}{L_s^*} = \sqrt{1 + \beta^2 \frac{\tau_s^*}{\tau^*}} - \beta \sqrt{\frac{\tau_s^*}{\tau^*}}, \qquad (16)$$

where $2\beta = \xi^*/\sqrt{1-\xi^*}$. One can show that $\mathscr{L}_s < L_s^*$ except for a large spin relaxation ($\tau_s^* << \tau^*$) in which case one has $\mathscr{L}_s \approx L_s^*$. This implies that, because of the spin-charge coupling mechanism, spin diffusion is also to some extent blocked by the photovoltage. However, the effective spin diffusion constant, defined as $\mathscr{D}_s = \mathscr{L}_s^2/\tau_s^*$, is in the general case larger than the usual photovoltage-free diffusion constant D_e. Fig. 5. shows that, depending on the value of ξ and $\tau_s^* << \tau^*$, the ratio $\mathscr{D}_s/\mathscr{D}_e$ can be as large as one order of magnitude. Using the experimental value of $\xi^* = 0.8$ and the estimated value of $\tau_s^* << \tau^*$ (see arrow in Fig. 5), one finds $\mathscr{D}_s/\mathscr{D}_e \approx 1.4$ and $\mathscr{L}_s \approx 2.3$ μm, which is, within experimental accuracy, close to the measured value of 2.9 μm.

IV. CONCLUSION

In summary, it has been shown that, if a sample with an open surface is excited by a tightly-focused laser beam, lateral charge diffusion is likely to be blocked by the spatially-dependent surface photovoltage. This can lead to a strong reduction of the minority carrier diffusion constant (we find experimentally a factor of 5). The lateral variation of the photovoltage induces a spin-charge coupling mechanism, due to which the spin diffusion is also decreased, but much less than charge diffusion. This results, even if spin relaxation cannot be neglected, in a spin diffusion length comparable with the charge one, and in a spin diffusion constant larger than the charge one. These results are of interest for all studies of charge and spin diffusion in bulk semiconductors or nanowires which are not covered by a passivating overlayer.

Acknowledgments

We are grateful to K. Lahlil for assistance in the chemical surface passivation. One of us (V. L. B.) is grateful to IDEX Paris-Saclay for funding his research stay.

[1] D. Luber, F. Bradley, N. Haegel, M. Talmadge, M. Coleman, and T. Boone, Appl. Phys. Lett **88**, 163509 (2006).
[2] G. D. Gilliland, M. S. Petrovic, H. P. Hjalmarson, D. J. Wolford, G. A. Northrop, T. F. Kuech, L. M. Smith, and J. A. Bradley, Phys. Rev. B **58**, 4728 (1998).
[3] I. Favorskiy, D. Vu, E. Peytavit, S. Arscott, D. Paget, and A. C. H. Rowe, Rev. Sci. Instr. **81**, 103902 (2010).
[4] F. Cadiz, P. Barate, D. Paget, D. Grebenkov, J. P. Korb, A. C. H. Rowe, T. Amand, S. Arscott, and E. Peytavit, J. Appl. Phys. **116**, 023711 (2014).
[5] S. A. Crooker and D. L. Smith, Phys. Rev. Lett **94**, 236601 (2005).
[6] R. Volkl, M. Griesbeck, S. A. Tarasenko, D. Schuh, W. Wegscheider, C. Shuller, and T. Korn, Phys. Rev. B **83**, 241306 (2011).
[7] T. Henn, T. Kiessling, W. Ossau, L. W. Molenkamp, D. Reuter, and A. D. Wieck, Phys. Rev. B **88**, 195202 (2013).
[8] F. Cadiz, D. Paget, A. C. H. Rowe, V. L. Berkovits, V. P. Ulin, S. Arscott, and E. Peytavit, J. Appl. Phys. **114**, 103711 (2013).
[9] D. Paget, A. O. Gusev, and V. L. Berkovits, Phys Rev B **53**, 4615 (1996).
[10] D. Paget, F. Cadiz, A. C. H. Rowe, F. Moreau, S. Arscott, and E. Peytavit, Journal of Applied Physics **111**, 123720 (2012).
[11] D. Vu, S. Arscott, R. Ramdani, E. Gil, Y. André, S. Bansropun, B. Gérard, A. C. H. Rowe, and D. Paget, Phys. Rev. B **82**, 115331 (2010).
[12] R. J. Nelson and R. G. Sobers, J. Appl. Phys. **49**, 6103 (1978).
[13] K. Zerrouati, F. Fabre, G. Bacquet, J. Bandet, J. Fran-

don, G. Lampel, and D. Paget, Phys. Rev. B **37**, 1334 (1988).
[14] H. Hasegawa, M. Akazawa, A. Domanowska, and B. Adamowicz, Appl. Surf. Sci. **256**, 5698 (2010).
[15] F. Cadiz, V. Notot, J. Filipovic, D. Paget, C. P. Weber, L. Martinelli, A. C. H. Rowe, and S. Arscott, J. Appl. Phys. **122**, 095703 (2017).